Ahmed S. Ahmed [1]
Yasir A. Ali [2]
Hyder A. Salih [2]
Khaleel I. Hassoon [2]
Younis M.A. Al-zahy [3]

[1] Department of Physics, College of Science, Misan University, Misan, IRAQ
[2] College of Applied Sciences, University of Technology, Baghdad, IRAQ
[3] Department of Physics, College of Education, Misan University, Misan, IRAQ

Spectroscopy of Copper/Zinc Alloys Plasma Generated by Laser

In this work, atmospheric plasmas are produced from different Cu-Zn alloys by Nd:YAG laser. Three copper alloys with different zinc rations, namely Cu80-ZnE100, Cu74-ZnE100 and Cu68-ZnE100 are examined. The Boltzmann plot approach and the Stark broadening technique are utilized to determine the electron temperature and plasma density for the induced plasma by laser. The electron temperature for the Cu80-ZnE100 and Cu74-ZnE100 plasmas is enhanced by 0.78 eV, and the electron density is increased from 7.6×10^{15} cm^{-3} to 9.4×10^{15} cm^{-3} when the laser beams hit the samples, while, the electron temperature in the Cu68-ZnE100 plasma is enhanced to 0.83 eV, and the density is increased to 1.29×10^{16} cm^{-3}.

Keywords: Laser-Induced breakdown; Saha-Boltzmann equation; Plasma temperature **Received:** 16 January 2025; **Revised:** 6 April; **Accepted:** 13 April 2025

1. Introduction

The development of high-intensity laser sources has, among other things, created new opportunities in the elemental analysis of solids, liquids, and gases [1]. The basic premise is that the various atomic and molecular forms can be inferred from the spectral emission resulting from vaporizing and exciting an absorbing material (whether a gas, liquid, or solid) with a laser pulse of the right intensity [2]. A very versatile laser-based diagnostic tool, laser-induced breakdown spectroscopy (LIBS), has several potential uses3. A concentrated, high-powered laser beam can quickly raise the temperature of a small area or spot on a solid surface to the point where the material vaporizes, creating an optically generated plasma [3]. In recent times, LIBS has been suggested for use in materials science, environmental protection, industrial process control, and the conservation and study of cultural heritage [4]. In the LIBS, the spectral signature of an analyte in plasma created by a high-irradiance pulsed laser is collected and processed [5,6]. The characteristics of laser-induced plasma are affected by various factors, including the characteristics of the target, the properties of the ambient medium, the laser wavelength, and pulse duration [7]. As a potential replacement or addition to Inductively Coupled Plasma (ICP) diagnostics, the LIBS has been used already in various diagnostic applications, such as studying solid samples and using an emissivity analysis of the plasma plume generated by the laser interaction with a solid surface to determine the essential concentrations of components [1,8]. The plasma in LIBS is often optically dense and thermally inelastic. There is a substantially higher temperature in the plasma center than in the plasma peripheral because of the laser material contact [9]. Laser-Induced Breakdown Spectroscopy (LIBS) is a valuable analytical method because it can generate plasma on untreated samples. The only requirement is optical accessibility, with optical fibers used for detection [10,11]. LIBS analyses of both bulk and nanostructured materials offer insights into crystallite size, purity, and shape, complementing data obtained from various spectroscopic and microscopic techniques. Information obtained from LIBS can be correlated with results from other methods like X-ray, scanning electron microscopy (SEM), and energy-dispersive X-ray analysis. However, despite its significance, techniques like X-ray diffraction (XRD) and SEM are more frequently employed [12-14].

2. Theoretical Background

Spectroscopic data interpretation necessitates a model of plasma ionization that describes the state of ionization and populations of atoms and ions at different energy levels in terms **o**f the temperature of plasma and the density of electron. And, the procedures to find the optically thin as well as the (LTE) plasma LIP parameters (T) and (n_e) are detailed below.

2.1 Boltzmann plot method for (T)

The distribution law of Boltzmann provides the population of species' energy levels for plasma in LTE is given by [15,16],

$$\frac{n_{k,Z}}{n_Z} = \frac{g_{k,Z}}{P_Z} exp\left(-\frac{E_{k,Z}}{k_B T}\right) \quad (1)$$

where n_z represents the total number density (or population), P_z is the partition function for species Z. The state of the ionization of a species, k_B, T, $n_{k,Z}$, $E_{k,Z}$, $g_{k,Z}$ that are corresponding to the Boltzmann constant, plasma temperature, population, energy, and

degeneracy of the upper energy level k in the optically thin plasma (OTP), where the minimum radiation being absorbed, is expressed as [17]:

$$I_Z = \frac{hc}{4\pi\lambda_{ki,Z}} A_{ki,Z} n_{k,Z} L \quad (2)$$

where, h denotes the constant of Planck constant, c represents the light speed, $A_{ki,Z}$ indicates the probability of transition, $\lambda_{ki,Z}$ refers to the transition line wavelength, and L signifies the plasma distinctive length,. By employing equation (1), equation (2) can be reformulated as [18]:

$$I_Z = \frac{hc}{4\pi\lambda_{ki,Z}} A_{ki,Z} L \frac{n_Z}{P_Z} g_{k,Z} \exp\left(-\frac{E_{k,Z}}{k_B T}\right) \quad (3)$$

Taking the natural logarithm of equation (3) allows it to be rewritten as:

$$ln\left(\frac{I_Z \lambda_{ki,Z}}{g_{k,Z} A_{ki,Z}}\right) = -\frac{1}{k_B T} E_{k,Z} + ln\left(\frac{hcLn_Z}{4\pi P_Z}\right) \quad (4)$$

This produces a linear graph, known as the plot of Boltzmann, where the magnitude of various transitions versus the upper level energy of species at the stage of ionization (Z) is plotted on the left side. Also, the temperature value is derived from the Boltzmann plot's slope. Equation (4) is derived beneath the assumptions of an (OTP) and local thermodynamic equilibrium (LTE), so its applicability is confined to the OTP and the LTE.

2.2 Method of Saha-Boltzmann Equation for n_e

Saha-Boltzmann equation can be used to determine the electron density in plasma if some conditions are satisfied (1) Thermodynamic equilibrium, (2). Initial electron density and partition functions can be theoretically estimated for ions, (3) The plasma should be optically thin and homogeneous plasma, and (4) Time-resolved measurements and calibration with standards. In our setup, all these condition are satisfied.

The condition for optically thin plasma is also satisfied since the optical sensor is immersed inside the plume and hence the emitted radiation can be detected without significant absorption or scattering.

Using Saha-Boltzmann equation, the electron density may be calculated from the plasma's atom and ion spectral lines as:

$$n_e = \frac{I_Z^*}{I_{Z+1}^*} 6.04 \times 10^{21} (T)^{\frac{3}{2}} \times \exp\left[\frac{(-E_{k,Z+1} + E_{k,Z} - \chi_Z)}{k_B T}\right] cm^{-3} \quad (5)$$

where, $I_Z^* = I_Z \lambda_{ki,Z} / g_{k,Z} A_{ki,Z}$ and χ_Z are the species' ionization energy in the stage of ionization (Z). And, the ionization energy lowering owing to the plasma interactions is unimportant slightly which being omitted into Eq. (5).

2.3 Optically thin plasma (OTP)

Determining elemental composition through line intensities in LIBS is simple when the plasma is optically thin and in Local Thermodynamic Equilibrium (LTE). It is essential to comprehend the time window of laser-induced plasmas under these circumstances. The intensity ratio for the same species at a given ionization stage (Z) is described by Eq. (6).

$$\frac{I_1}{I_2} = \left(\frac{\lambda_{nm,Z}}{\lambda_{ki,Z}}\right)\left(\frac{A_{ki,Z}}{A_{nm,Z}}\right)\left(\frac{g_{k,Z}}{g_{n,Z}}\right) \exp\left(-\frac{E_{k,Z} - E_{n,Z}}{k_B T}\right) \quad (6)$$

I_1 is the line intensity corresponding to the transition from k to i-state, and I_2 represents the intensity corresponding the transition from n to m-state. It is essential to regard the (2) lines of emission with the similar or closely related higher levels.

Although the minimum requirement for measuring the temperature is the two spectral lines, but the Boltzmann plot provides more accurate measurement of temperature, because it considers the multiple spectral lines. Tables (1) and (2) evince the parameters of the spectral lines used in drawing the Boltzmann plot. The electron temperature (T_e) in this paper is calculated from the relative intensities of the observed lines. The influence of temperature, as described via the parameter of Boltzmann upon the ratio of line intensity reproducibility is reduced. In contrast, the efficiency factor of collecting system is not considered. By disregarding the exponential parameter in that state, the intensity ratio's theoretical value of both lines can be determined employing the transitions atomic factors. By examining this ratio against measured values at various deferral times, we can determine when the plasma is optically thin.

The Boltzmann distribution law predicts that many ground-state atoms will remain in the plasma's periphery, where the temperatures are low. It provides the populations of the energy level of species for plasma in the local thermodynamic equilibrium (LTE) [18]:

$$I_{ki} = \frac{hc}{4\pi\lambda_{ki}} A_{ki} g_j \frac{N}{Z} e^{-E_k/k_B T} \quad (7)$$

The effectiveness of LIBS as an analytical approach has been aided by research into both applications and a fundamental understanding of the essential LIBS processes, although particular hurdles remain in performing nanoparticle analysis. The complexity of plasma–particle interactions and the nature of the LIBS plasma make it challenging to analyze the nanoparticles [19, 20]. The development of LIBS aims to enhance its quantitative analytical capabilities, focusing on improving measurement precision and accuracy for specific applications. Analyzing steel and its alloys with LIBS is complicated by spectrum interference from emission lines, where the lines in the desired spectral region overlap with various emission lines from the components being analyzed, causing deviations in the spectra from their baseline. This can sometimes lead to poor-quality analysis when using univariate regression models [21]. Cirisan et al. explored the structure and dynamics of the plasma plume generated in open air by a nanosecond laser beam impact on metallic objects through fast photography and numerical simulations [22]. In a study led by Hanif and colleagues, a Q-switched Nd:YAG

laser was employed to examine the titanium plasma created when the laser hit a solid titanium target in open air. The research revealed that electron temperature and density are highest at the target's surface and decrease as the distance from the target grows. Variations in these plasma properties with different laser energies indicate a proportional increase in electron temperature and density with higher laser power [23]. Karki et al. [21] performed an elemental analysis of high alloy steels using six distinct normalization methods to determine the most effective technique for identifying present elements. Sherbini et al. [24] investigated the optical breakdown at nanostructured target materials generated by an Nd:YAG laser device and studied the effects of nanoparticle size, laser wavelength and fluence, and time delay on the strength of the nanomaterial signals. Ali et al. [25] studied the plasma generated by nano and bulk copper targets by using a 1064 nm Nd:YAG pulsed laser. Since the high-energy photons absorbed by nano copper targets have a larger surface area and a greater penetration depth than bulk copper targets, and more energy can be transmitted within the nanomaterial, raising the plasma's temperature. This is partly due to the increased depth of the penetration of laser energy and the large surface area of these materials.

3. Experimental Setup

In this study, a plasma generated from copper alloys using an Nd:YAG laser (1064 nm) was analyzed through the LIBS technique. An Nd:YAG laser (HuaFei TongDa Technology – Diamond -288 Pattern EPLS) with a wavelength of 1064 nm, a pulse duration of 9 ns, and a pulse energy range of 100-1000 mJ was used to produce the plasma. Copper alloys Cu80Zn, Cu74Zn, and Cu68Zn, each sized at 1×1 cm², served as the target materials. To direct the laser beam onto the target, a convex lens with a focal length of 20 cm was employed, focusing the laser pulses at atmospheric pressure. The target surface was manually rotated after each laser shot to ensure uniform plasma formation. Figure (1) depicts the LIBS setup utilized in this research, highlighting the importance of the laser and optical spectrometer in the apparatus.

The emission from the ablation laser beam was collected axially using 2-mm diameter optical fibers, as illustrated in Fig. (1).

4. Results and Discussion

The wavelength range of 500-530 nm was used to record the emission spectra of Cu80ZnE100, Cu74-ZnE100 and Cu68-ZnE100 alloys from the excited and ionic atoms. The NIST database was utilized to allocate all the detected line locations properly. Figure (2) depicts the Boltzmann plot that based on the intensity of each spectral line for Cu80ZnE100 alloy. The relationship is a straight line, its slope according to Eq. (1) gives the temperature of plasma electrons which is for this case T = 0.78 eV. The estimated values of plasma parameters for Cu-ZnE100 alloy are shown in table (3).

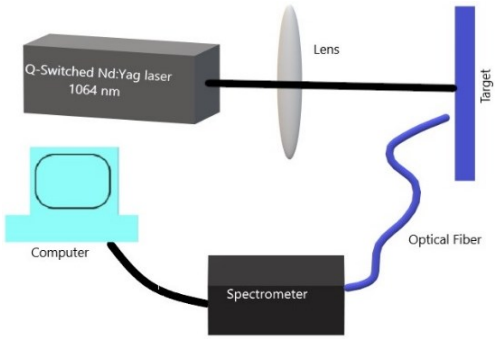

Fig. (1) Experimental setup for LIBS

In all cases, the most important factor influencing the values of the electron temperature and the electron number density is the laser power. Intensity-based Boltzmann plots of Cu74ZnE100 and Cu68ZnE100 alloys are shown in figures (3) and (4), respectively. The electron temperature and the electron number density are determined to be 0.78, 0.83 eV and 9.42×10^{15}, 1.29×10^{16} cm^{-3} for Cu74-ZnE100 and Cu98-ZnE100, respectively.

The density of electrons can be calculated from a specific spectral line, as indicated in figures (5), (6) and (7), which reveal that the spectral line for the copper atom has Lorentzian profile with half-width broadening ($\Delta\lambda_{1/2}$) given by [26,27]:

$$\Delta\lambda_{1/2} = 2w\left(\frac{N_e}{10^{16}}\right) + 3.5A^4\sqrt{\left(\frac{N_e}{10^{16}}\right)}\left[1 - \frac{3}{4}\mathrm{n}^{-1/3}\right]w\left(\frac{N_e}{10^{16}}\right) \quad (8)$$

where $\Delta\lambda_{1/2}$ represents the Stark broadening, A is the ion broadening, w is the impact width of electron and n is the particles volume density in the Debye sphere

The experimental results showed that the intensity of Cu80-Zn is about (0.55 a.u.) at the wavelength value (521.8 nm), similar to the case of Cu68-Zn, whereas this intensity enhancement reduces to around (0.4 a.u.) at the Cu74-Zn. The possible explanations for this finding include the plasma shielding effects of irradiation.

The observed variation in the emission intensity, electron temperature, and electron number density between these three cases depends on the plume growth's hydrodynamics.

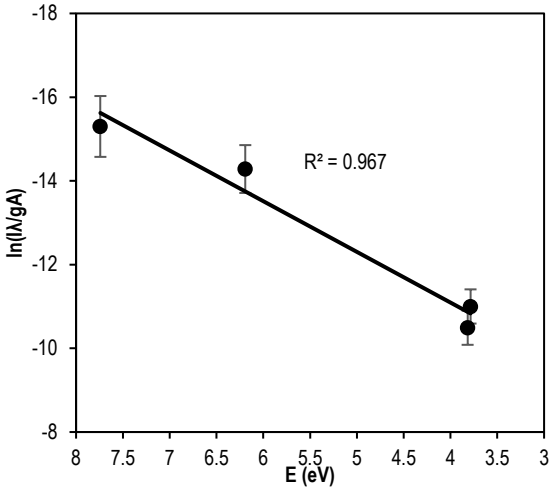

Fig. (2) The Boltzmann plot with best straight line fit for Cu80ZnE100 Alloy

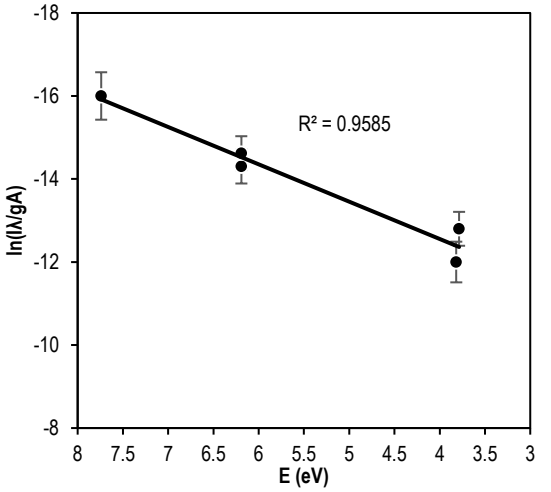

Fig. (3) The Boltzmann plot with best straight line fit for Cu74.9ZnE100 alloy

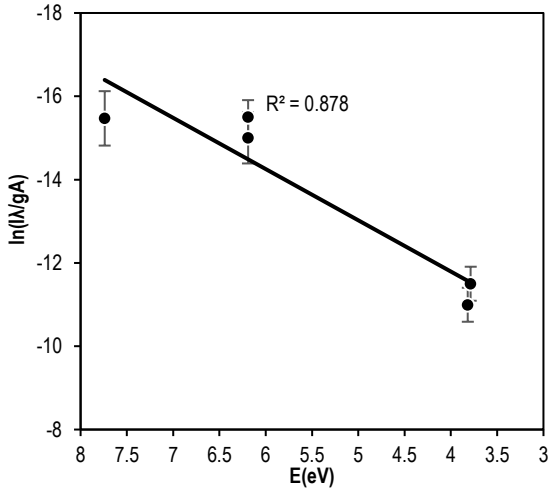

Fig. (4) The Boltzmann plot with best straight line fit for Cu68ZnE100 alloy

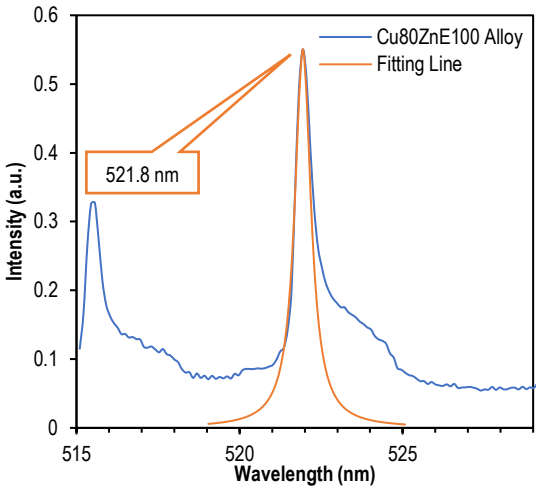

Fig. (5) The Lorentz fitting process for the spectral line of Cu80ZnE100 alloy plasma at wavelength of 521.8 nm

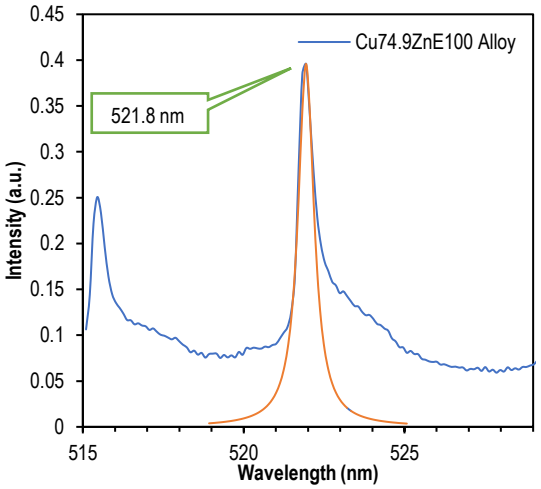

Fig. (6) The Lorentz fitting process for the spectral line of Cu74.9ZnE100 alloy plasma at wavelength of 521.8 nm

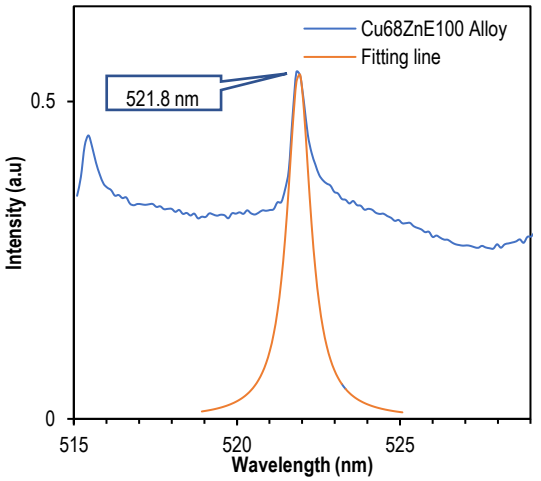

Fig. *(7)* The Lorentz fitting process for the spectral line of Cu68ZnE100 Alloy plasma at wavelength of 521.8 nm

5. Conclusions

This study employed Nd:YAG laser to produce plasma from several targets of CuZn alloys with different Zn ratios. The absorption of high-energy photons leads to an increase in the electrons' kinetic energy, which in turn results as a variation in their plasma temperature. For the same laser energy, it is also shown that plasma temperatures are varied amongst different CuZn alloys. At identical laser energy levels, differing electron densities are observed in targets because of the quantum mechanical characteristics of the materials. Under identical operation conditions, the the rates of increment and reduction in plasma parameters (T_e, N_e, ω_p, and λ_D), vary with the Zn ratio in the CuZn alloys.

References

[1] A.W. Miziolek, V. Palleschi and I. Schechter, **"Laser induced breakdown spectroscopy"**, Cambridge University Press (2006).

[2] A.M. Malvezzi, "Laser–Matter Interaction in LIBS Experiments", in **Laser-Induced Breakdown Spectroscopy**, Springer (2014), pp. 3-29.

[3] K. Song, Y.-I. Lee and J. Sneddon, "Applications of Laser-Induced Breakdown Spectrometry", *Appl. Spectro. Rev.,* 32(3) (1997) 183-235.

[4] A. Bertolini et al., "Modì: a new mobile instrument for in situ double-pulse LIBS analysis," *Anal. Bioanal. Chem.,* 385(2) (2006) 240-247.

[5] D. Mukherjee, A. Rai and M. Zachariah, "Quantitative laser-induced breakdown spectroscopy for aerosols via internal calibration: Application to the oxidative coating of aluminum nanoparticles", *J. Aerosol Sci.,* 37(6) (2006) 677-695.

[6] S.N. Mazhir et al., "The effect of gas flow on plasma parameters induced by microwave", *Baghdad Sci. J.,* 15(2) (2018) 0205-0205.

[7] N.M. Saadoon, N.M. Hadi and S.H. Sahaah, "Nanomaterial and Laser Induced–Breakdown Spectroscopy (LIBS)", *J. Univ. Babylon Pure Appl. Sci.,* 27(5) (2019) 294-306.

[8] F. Capitelli et al., "Determination of heavy metals in soils by laser induced breakdown spectroscopy", *Geoderma,* 106(2) (2002) 45-62.

[9] J.-M. Li et al., "Self-absorption reduction in laser-induced breakdown spectroscopy using laser-stimulated absorption", *Opt. Lett.,* 40(22) (2015) 5224-5226.

[10] S.M. Angel et al., "LIBS using dual- and ultra-short laser pulses", *Fresenius' J. Anal. Chem.,* 369(3) (2001) 320-327.

[11] K.A. Aadim, "Spectroscopic study for plasma parameters in co-sputtering system", *Iraqi J. Phys.,* 14(31) (2016) 122-128.

[12] H.M. Fadhil, K.I. Hassoon and H.A. Salih, "Structural and Spectroscopic Analysis for Silver Bulk and Nanoparticles", *Karbala Int. J. Mod. Sci.,* 8(2) (2022) 52-62.

[13] Q.A. Abbas, "Influence of working pressure and lasing energy of Al plasma in laser-induced breakdown spectroscopy", *Iraqi J. Phys.,* 17(40) (2019).

[14] N.K. Abdalameer and S.N. Mazhir, "Laser-Induced Plasma Atomic and Ionic Emission during Target Ablation", *Int. J. Nanosci.,* 20(05) (2021) 2150044.

[15] H.R. Griem, **"Principles of Plasma Spectroscopy",** Cambridge University Press (2005).

[16] A.H. Shaker, K.A. Aadim and M.H. Nida, "Spectroscopic analysis of zinc plasma produced by alternating and direct current jet", *J. Optics,* 53(2) (2024) 1273-1281.

[17] Q.A. Abbas, A.F. Ahmed and F.A.-H. Mutlak, "Spectroscopic analysis of magnetized hollow cathode discharge plasma characteristics", *Optik,* 242 (2021) 167260.

[18] V. Unnikrishnan et al., "Measurements of plasma temperature and electron density in laser-induced copper plasma by time-resolved spectroscopy of neutral atom and ion emissions", *Pramana Indian J. Phys.,* 74 (2010) 983-993.

[19] P.K. Diwakar et al., "Laser-induced breakdown spectroscopy for analysis of micro and nanoparticles", *J. Anal. Atomic Spectromet.,* 27(7) (2012) 1110-1119.

[20] M.A. Ismail et al., "LIBS limit of detection and plasma parameters of some elements in two different metallic matrices", *J. Anal. Atomic Spectromet.,* 19(4) (2004) 489-494.

[21] V. Karki et al., "Comparison of spectrum normalization techniques for univariate analysis of stainless steel by laser-induced breakdown spectroscopy", *Pramana Indian J. Phys.,* 86(6) (2016) 1313-1327.

[22] M. Cirisan et al., "Laser plasma plume structure and dynamics in the ambient air: The early stage of expansion", *J. Appl. Phys.,* 109(10) (2011) 103301.

[23] M. Hanif, M. Salik and M. Baig, "Optical spectroscopic studies of titanium plasma produced by an Nd:YAG laser", *Opt. Spectro.,* 114(1) (2013) 7-14.

[24] A.E. Sherbini et al., "Nano-particle enhancement of diagnosis with Laser-Induced plasma spectroscopy", *J. Phys.: Conf. Ser.*, 1253(1) (2019) 012002.

[25] Y.A. Ali and R.A. Khamis, "Spectroscopic Study of Copper Plasma Produced by Nd:YAG Laser from The Nano and Bulk Copper Targets", *J. Phys.: Conf. Ser.*, 1818(1) (2021) 012008.

[26] A. Khalil et al., "Titanium plasma spectroscopy studies under double pulse laser excitation", *Laser Phys.,* 19(10) (2009) 1981-1992.

[27] H.M. Fadhil, H.A. Salih and K.I. Hassoon, "Spectroscopic and Structural Analysis of Aluminum Bulk and Nanoparticles: A Comparative Study", *J. Appl. Sci. Nanotech.,* 2(3) (2022) 85-94.

Table (1) Wavelength, lower and upper energy levels, upper level degeneracy and transition probability for the Cu74-Zn emission lines utilized in the present work

Atom/Ion	Wavelength (nm)	NIST Data	Higher level of Energy (eV)	Lower level of Energy (eV)	Probability of Transition	Higher level of Degeneracy (s^{-1})
Cu II	342.86	342.87	17.263	13.648	-	3
Cu I	510.7	510.55	3.817	1.389	2.00E+06	4
Cu I	515.447	515.323	6.191	3.785	6.00E+07	4
Cu I	521.94	521.82	6.192	3.816	7.50E+07	6
Cu I	578.403	578.213	3.785	1.642	1.65E+06	2
Cu II	589.781	589.797	16.563	14.462	-	7
Zn	334.403	334.501	7.783	4.077	1.70E+08	7
Zn	396.183	396.543	8.921	5.795	-	5
Zn	468.123	468.143	9.296	6.654	-	3
Zn	472.242	472.215	6.654	4.029	-	3
Zn	481.187	481.053	6.654	4.077	-	3

Table (2) Wavelength, lower and upper energy levels, upper level degeneracy and transition probability for the Cu80-Zn emission lines utilized in the present work

Atom/Ion	Wavelength (nm)	NIST Data	Higher level of Energy (eV)	Lower level of Energy (eV)	Probability of Transition	Higher level of Degeneracy (s^{-1})
Cu I	405.779	405.678	6.871	3.816	-	8
Cu I	510.7	510.55	3.817	1.389	2.00E+06	4
Cu I	515.447	515.323	6.191	3.785	6.00E+07	4
Cu I	521.939	521.82	6.192	3.816	7.50E+07	4
Cu II	578.403	578.392	17.43	15.287	-	1
Zn	472.3	472.215	6.654	4.029	-	3
Zn	481.187	481.053	6.654	4.077	-	3

Table (3) Plasma parameters for Cu-ZnE100 alloy

	T_e (ev)	N_e (cm^{-3})	F_p(Hz)	λ_d (cm)	N_d
Cu80-Zn	0.7886	7.60E+15	7.83E+11	7.57E-06	1.38E+01
Cu74-Zn	0.7830	9.42E+15	8.72E+11	6.77E-06	1.23E+01
Cu68-Zn	0.8330	1.29E+16	1.02E+12	5.97E-06	1.15E+01

